

www.acsnano.org

Effects of Layering and Supporting Substrate on Liquid Slip at the Single-Layer Graphene Interface

Gus Greenwood, Jin Myung Kim, Qianlu Zheng, Shahriar Muhammad Nahid, SungWoo Nam,* and Rosa M. Espinosa-Marzal*



Cite This: ACS Nano 2021, 15, 10095-10106



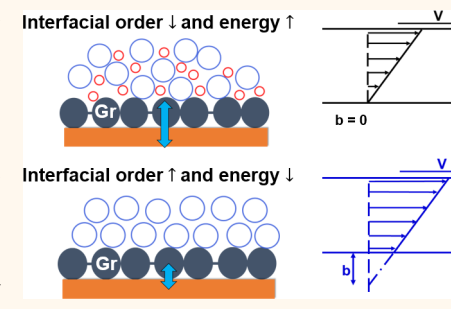
ACCESS

III Metrics & More

Article Recommendations

Supporting Information

ABSTRACT: Understanding modulation of liquid molecule slippage along graphene surfaces is crucial for many promising applications of two-dimensional materials, such as in sensors, nanofluidic devices, and biological systems. Here, we use force measurements by atomic force microscopy (AFM) to directly measure hydrodynamic, solvation, and frictional forces along the graphene plane in seven liquids. The results show that the greater slip lengths correlate with the interfacial ordering of the liquid molecules, which suggests that the ordering of the liquid forming multiple layers promotes slip. This phenomenon appears to be more relevant than solely the wetting behavior of graphene or the solid—liquid interaction energy, as traditionally assumed. Furthermore, the slip boundary condition of the liquids along the graphene plane is sensitive to the substrate



underneath graphene, indicating that the underlying substrate affects graphene's interaction with the liquid molecules. Because interfacial slip can have prominent consequences on the pressure drop, on electrical and diffusive transport through nanochannels, and on lubrication, this work can inspire innovation in many applications through the modulation of the substrate underneath graphene and of the interfacial ordering of the liquid.

KEYWORDS: slip, graphene, transition state, substrate-induced doping, friction, interfacial structure

🕇 he assumption of a no-slip boundary condition lies near the heart of traditional fluid dynamics, where making that assumption allows for the classical mathematical description of fluid flow. As measurement techniques gain increased resolution, and nanoscale systems find popularity and growing applications, experimental evidence and theory indicate that there is indeed slip at the interface between many liquids and surfaces at the nanoscale. This slip condition is commonly quantified using the concept of a slip length, b, which describes the distance away from the assumed surface at which the fluid velocity profile reaches zero (see the lower inset of Figure 1A). A positive slip length indicates a nonzero, positive fluid velocity at the surface—i.e., the extrapolated profile reaches zero below the surface correlating with the decreased strength of interactions between the surface and liquid molecules and an enhanced flow. The slip length is affected by the structure and density of the liquid at the interface, surface curvature or structure, and solid-liquid interaction.² Interfacial slip affects flow in micro- and nanomechanical/fluidic systems, lubrication, and confined biological, industrial, and technological processes, such as the flow of electrolytes in porous electrodes, particle aggregation, and sedimentation, making it not only of fundamental relevance but also critical for applications.

One family of surfaces that has gained popularity toward the end of foundational slip length studies is that of few-layer carbonaceous materials. In particular, the ultrafast flow through carbon nanotubes has been primarily attributed to a large slip length, therefore creating interest in the fundamental drivers of the slip phenomenon in carbonaceous systems. At around the same time, graphene, a single atomic layer of hexagonally bonded carbon, was isolated and became an intense focus of study. The electronic properties of graphene served as the initial focus of investigation, but its interactions with liquids were also studied (see ref 6 for a recent thorough review of the topic). Despite the rapid broadening of graphene research in recent years, there is still a lack of molecular level

Received: March 3, 2021 Accepted: June 4, 2021 Published: June 11, 2021





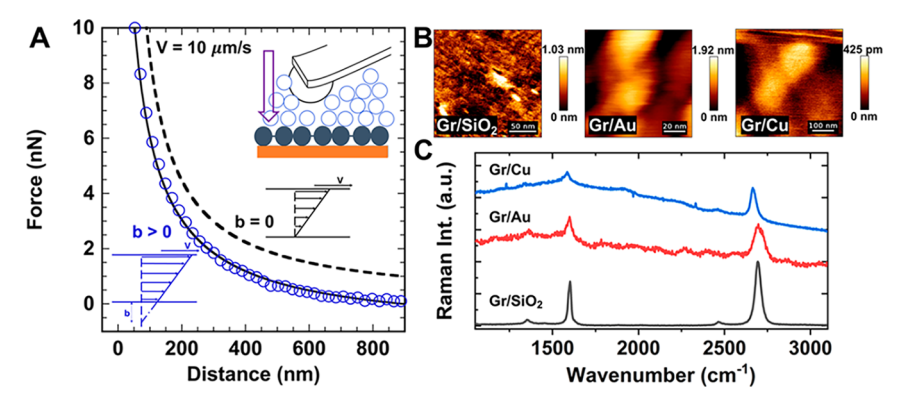


Figure 1. Experimental approach to measuring slip length on prepared graphene surfaces. (A) Representative force profile for the hydrodynamic drag force on a silica microsphere approaching a Gr/Cu surface as measured by AFM. Open blue circles are the measured force in the ionic liquid EMIM FAP at an approach velocity of $10 \, \mu m/s$, and the solid black line is the fit to eq 2. The dashed black line shows the theoretically expected force calculated using experimental conditions and a slip length of b=0 nm. The fluid velocity profiles for a generic Couette flow under partial-slip and no-slip conditions are shown in blue and black insets, respectively. The top-right inset is a cartoon, not to scale, of the experimental approach in a generic liquid (empty circles). Graphene, the gray circles, is supported by a copper substrate in this example. (B) Topography of annealed graphene on 285 nm thick SiO_2 , 100 nm thick Au, and Cu foil substrates measured by AFM. RMS roughnesses of these samples were estimated to be 0.2, 0.3, and 0.45 nm, respectively. (C) Raman spectra of annealed graphene on various substrates. Annealing on different substrates did not significantly change the intensity ratio between characteristic peaks of graphene (e.g., D peak at 1350 cm⁻¹, G peak at 1595 cm⁻¹, and 2D peak at 2690 cm⁻¹).

understanding of its interaction with liquids. In fact, while there are several simulation studies investigating the slip length of graphene (along with its conformations) and its controlling factors, very few studies have attempted to experimentally quantify the slip length of a smooth graphene surface in any liquid; those that have performed such measurements reported a very wide range of potential slip lengths for the same system. That wide range of slip length values was loosely attributed to differences in surface charge and substrate effects from variations between the different SiO₂ substrates used to support graphene, but there has been little to no additional experimental verification of the phenomenon since then. To the best of the authors' knowledge, experimental investigations of the slip length in graphene systems have remained inconclusive.

One goal of this work is to add to the experimental knowledge of slip length in single-layer graphene systems, specifically focusing on trends across liquids and on the influence of the graphene's support material, a characteristic of 2D materials. We use the well-established method of colloid probe atomic force microscopy (AFM)^{14,15} to directly measure the hydrodynamic force on a sphere approaching a flat graphene surface, allowing a quantitative determination of the slip length. These measurements are supplemented with nanoscale friction-force measurements using AFM equipped with a sharp tip, to quantify the molecular mobility of a liquid near a surface through modeling based on Eyring's transition state theory. By combining these approaches, we expand on the existing body of experimental slip length literature for graphene and present an alternative framework for interpreting, predicting, and controlling slip length.

RESULTS AND DISCUSSION

Single-layer graphene was used as-grown on the Cu foil (*i.e.*, without etching and transfer, referred to as Gr/Cu) and transferred to SiO_2 and Au substrates, labeled as Gr/Si and Gr/Au, respectively. We describe the graphene—substrate system with the nomenclature "Gr/x" indicating "single-layer graphene supported by substrate x". It is known that nanoscale

roughness can have significant effects on the slip length. ¹⁵ Although the same sample surface could not be used for all measurements, differences for Gr/Cu were mitigated by cutting the samples from the same large sheet of as-grown graphene. The root mean square (RMS) roughness as determined by AFM imaging was found to be less than 3 nm for all samples, and care was taken to restrict measurements to areas with a roughness smaller than ~1.8 nm. Representative AFM images are shown in Figure 1B. Raman spectra of graphene on various substrates in Figure 1C show that the intensity ratio of characteristic graphene Raman peaks (e.g., D at 1350 cm⁻¹, G at 1595 cm⁻¹, 2D at 2690 cm⁻¹) after annealing was not dependent on the underlying substrates, implying a similar quality of the graphene samples.

The hydrodynamic force on a silica microsphere was measured as it approached the graphene surface. The measurements on Gr/Cu were performed in seven different liquids (a sucrose 60 wt % aqueous solution, ethylene glycol, a silicone oil, and four ionic liquids) with different viscosity, polarity, and charge (see properties in Table S1), chosen to span a range of properties and to accommodate the sensitivity of our instrument. One of the ionic liquids, 1-ethyl-3methylimidazolium tris(perfluoroethyl)trifluorophosphate (abbreviated as EMIM FAP) and the sucrose solution (60 wt %) were also investigated on Gr/Au and Gr/Si. The silicon oxide microspheres were manually glued to tipless AFM cantilevers. While any sized sphere will work with this experimental approach in theory, we found spheres with diameters of ~ 18 μ m to strike a reasonable balance between measurable drag force and consistent sphere surface roughness. All slip length data shown in the main body of the paper were collected using the same microsphere and cantilever, but results were reproducible using other spheres and cantilevers. The measurements were performed at 5 approach velocities: 1, 3, 6, 10, and 20 μ m/s on smooth regions of the graphene surfaces based on AFM images.

The hydrodynamic force experienced by a sphere approaching a flat surface in liquid fulfilling $R\gg D$ is given by Reynold's lubrication theory 16,17

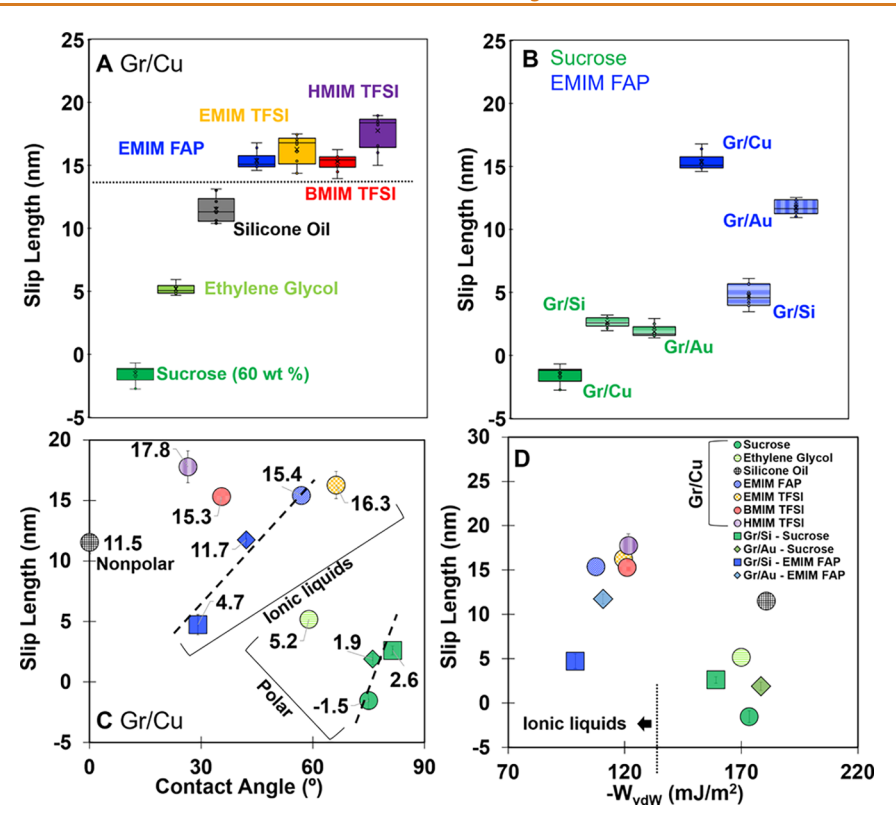


Figure 2. Measured slip lengths using a microsphere-equipped AFM cantilever. (A) Box and whisker plot of the slip length of 7 different liquids on Gr/Cu for a 6 μ m/s approach velocity. Each box includes ~10 separate measurements at the same location. (B) Slip lengths for the 60 wt % aqueous sucrose solution and EMIM FAP in contact with graphene supported by 3 different substrates. Each box includes ~10 separate measurements at the same location. (C) Slip length as a function of contact angle for each liquid, with the systems from part B included. Vertical and horizontal error bars represent the standard deviation of at least 10 individual slip length and contact angle measurements and are often too small to see. The dashed lines demonstrate the general increase of slip length with contact angle for a given liquid. (D) Slip length as a function of calculated van der Waals interaction energy for each system. Note that the x-axis does not start at 0. The legend in part D applies to part C as well. Values for reference measurements on silica surfaces are shown in Table S3 and Figure S1.

$$F_{\text{hyd}} = \frac{6\pi\eta R^2 \dot{D}}{D} \tag{1}$$

where $F_{\rm hyd}$ is the hydrodynamic drag force, η is the liquid's dynamic viscosity, R is the sphere radius, \dot{D} is the sphere's approach velocity, and D is the separation between the sphere and the surface. This simplified expression is acceptable in our experiments (R is 8.9 μ m, and D < 0.8 μ m), as proven in ref 18. While eq 1 assumes a slip length of 0, a modification that accounts for a nonzero slip length was introduced by Vinogradova¹

$$F_{\text{hyd}} = \frac{6\pi\eta R^2 \dot{D}}{D} f^* \tag{2}$$

where, for two surfaces of the same material (a chemically symmetric system) $^{18-20}$

$$f^* = \frac{D}{3b} \left[\left(1 + \frac{D}{6b} \right) \ln \left(1 + \frac{6b}{D} \right) - 1 \right]$$
 (3)

Positive values of b yield a hydrodynamic force experienced by the microsphere lower than the nonslip boundary condition. Negative b values reflect a change of sign of the fluid velocity field near the solid. The presence of surface-adsorbed liquid molecules that are effectively immobile and shift the location of zero velocity above the surface has been associated with a negative slip length (a stick length) as well. In the asymmetric systems composed of the silica colloid and the

graphene surface of this work, b is the average slip length of the two surfaces; this is the approach generally used when reporting slip lengths. We also used the less common method described in ref 19 to estimate the individual slip length along the graphene surface, b_1 , using b and the individual slip length on silica (b_2) obtained in reference measurements with a silica colloid approaching a naturally oxidized silicon wafer; see the Methods section.

Figure 1A shows a representative measurement. The upperright inset is a cartoon depiction of the system. The expected force profile as a function of distance described by eq 1 (when b=0) is shown with the dashed black line, while the force measured by AFM is shown with open blue circles. The measured data have been processed to ensure an accurate location of the surface and to account for the viscous drag of the cantilever (see the Methods section). The solid black line gives the fit of eq 2, with b>0 for EMIM FAP at $10~\mu m/s$.

Slip Length Dependence on Liquid Properties. Figure 2A shows the slip length on Gr/Cu at $V=6~\mu m/s$. Each box consists of approximately 10 individual slip length values measured at the same point on the Gr/Cu surface. Based on previous works, ¹⁸ accounting precisely for the drag force on the cantilever and the cantilever deflection and velocity are key to reliably determine the slip length (see the Methods section for a more detailed discussion). Slip lengths for the 5 selected velocities are shown in Table S2 and Figure S1 in the SI. The slip lengths in the investigated range of approach velocities do

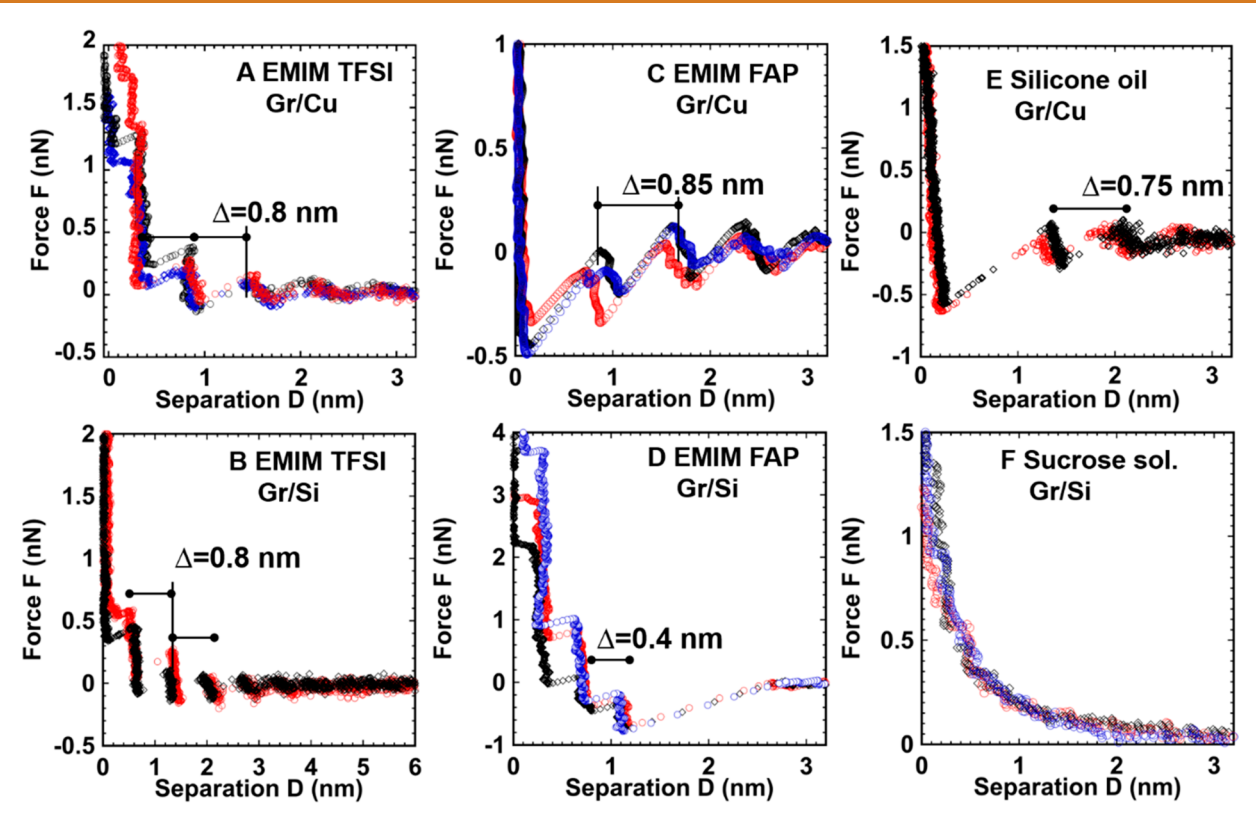


Figure 3. Structural force between graphene and an AFM tip in the liquids: EMIM TFSI on (A) Gr/Cu and (B) Gr/Si, EMIM FAP on (C) Gr/Cu and (D) Gr/Si, (E) silicone oil on Gr/Cu, and (F) sucrose solution on Gr/Si. The thickness of the layers is Δ , and it is shown in the diagrams to illustrate the liquid ordering. The measurements for ethylene glycol and sucrose solution on Gr/Cu demonstrate the presence of layers for ethylene glycol and no layers for sucrose solution, but the force is strongly adhesive (not shown), which hinders a precise analysis of the layer thickness. The results for ethylene glycol on Gr/Si illustrate the layering of this liquid very clearly (layer thickness $\Delta = 0.3$ nm); see Figure S6.

not depend on the approach velocity. In the main text, we show data only for the 6 μ m/s approach velocity for the purpose of comparison at a fixed condition.

The slip length varies dramatically depending on the liquid, and ionic liquids have clearly higher slip lengths (b > 15 nm) compared to other liquids (see the dashed line separating the slip lengths of ionic and nonionic liquids). Figure 2B shows b measured on graphene supported by three different substrates—copper, SiO_2 , and gold—in two different liquids, sucrose solution (green) and EMIM FAP (blue). The influence of the substrate underneath graphene on the slip length is significant for the two liquids.

Figure 2C shows the slip length vs contact angle θ relationship; details regarding the contact angle measurements can be found in the Methods section and the results in Figure S2. The contact angle results from the equilibrium between the interfacial energies (liquid-surface, surface-air, and liquidair) following Young's equation, and hence, it is a measure of solid-liquid interactions. It is immediately clear that the measured slip lengths do not follow the reported wettability trend for pure water of increasing slip length with increasing contact angle.²⁴ For example, negative slip lengths were obtained for sucrose solutions on Gr/Cu (e.g., -1.5 ± 0.7 at 6 μ m/s, $\theta = 75^{\circ}$), representing a condition of nonslip. Experiments by Honig and Ducker^{23,25} also showed no slip of sucrose solutions on OH-terminated (hydrophilic) and methyl-terminated silica glass ($\theta \sim 5-75^{\circ}$). Furthermore, the good agreement of our reference measurements on hydrophilic SiO₂ surfaces (Table S3 and Figure S1C₂D) with these results

supports that our experimental method and analysis are precise. On graphite, this previous work obtained slip lengths of the sucrose solution between 0 and 5 nm. However, it was attributed to the presence of step edges on graphite that led to a wrong estimation of the surface separation and thereby of the slip length. We do not have step edges on single-layer graphene, and hence, we do not believe that the obtained values of the slip length are associated with a wrong surface separation.

Although ethylene glycol and silicone oil wet graphene better than the sucrose solution ($\theta = 59$ and 0° for ethylene glycol and silicone oil, respectively, compared to 75° for sucrose solutions; Figure 2C), the slip lengths on Gr/Cu are greater (5.2 and 11.5 nm, respectively), compared to those of the sucrose solution, -1.5 nm. In the case of the four ionic liquids, higher slip lengths are observed (between 15.3 \pm 0.7 and 17.8 \pm 1.4 nm) in a range of contact angles with Gr/Cu ranging from 26.6 to 66.3°. Note that the same conclusions are inferred from the asymmetric analysis (Figure S3): b_1 is a bit higher than b for the ionic liquids, ethylene glycol, and silicone oil and a bit smaller than b for the sucrose solution. This emphasizes the nonslip condition for the sucrose solution, while b_1 indicates slip in the order EMIM FAP > EMIM bis(trifluoromethylsulfonyl)imide (TFSI) > 1-hexyl-3-methylimidazolium (HMIM) TFSI > 1-butyl-3-methylimidazolium (BMIM) TFSI > silicone oil > ethylene glycol.

Large slip lengths were found in simulations for a variety of fluids including water, decane, and ethanol at the interface with graphene. ²⁶ The simulation shows that the flow rates lie far

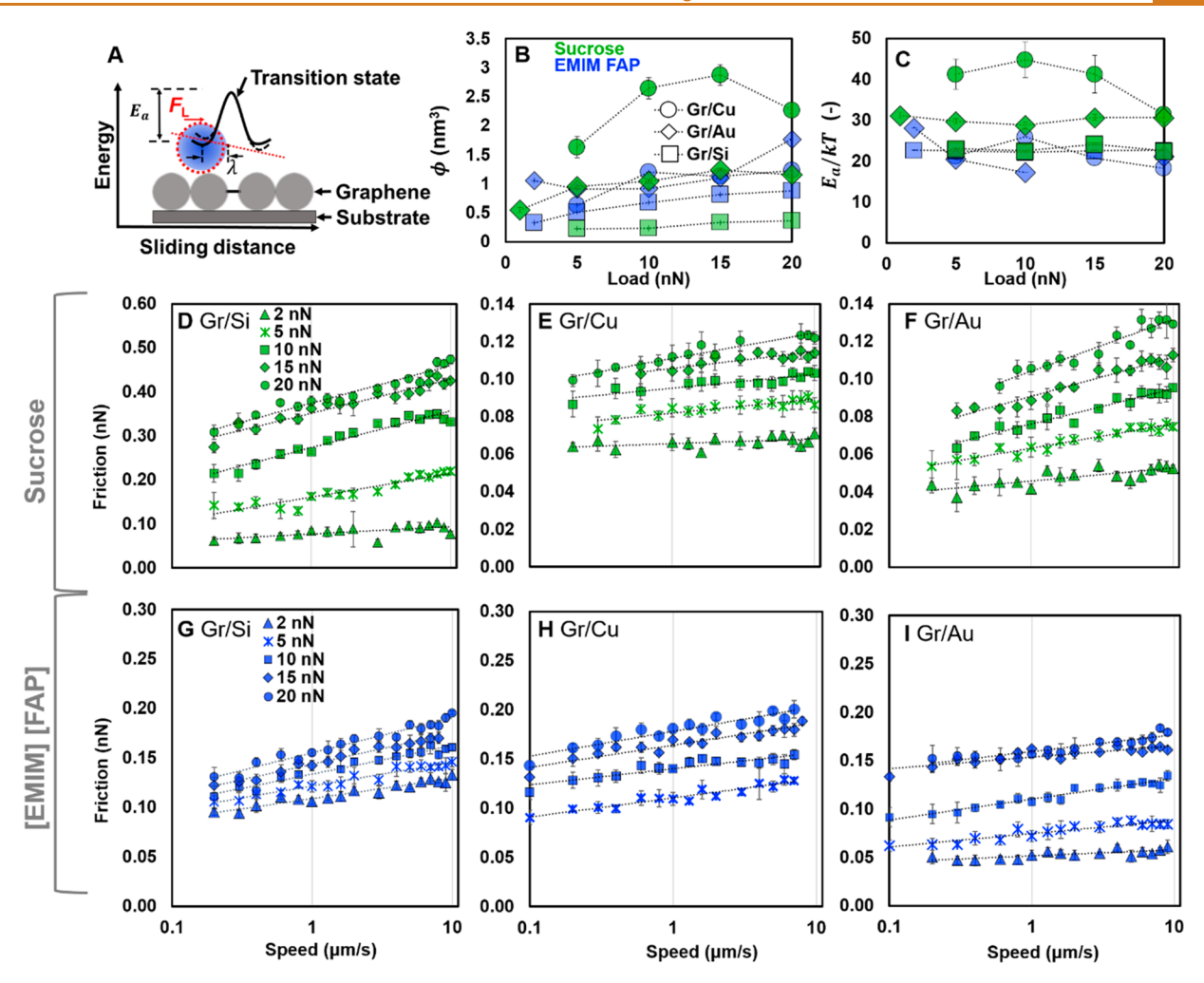


Figure 4. Friction measurements and analysis for 60 wt % sucrose and EMIM FAP on Gr/Cu, Gr/Si, and Gr/Au. (A) Cartoon representing Eyring's shear assisted thermally activated slip theory. (B) Shear activation volume and (C) activation energy for sucrose solution and EMIM FAP on Gr/Cu (circles), Gr/Au (diamonds), and Gr/Si (squares). Error bars are the standard deviation of 8 repeated scans. Panels D-F show results for the sucrose solution (green), and panels G-I are for the ionic liquid (blue) upon loads of 2, 5, 10, 15, and 20 nN (same legend for all panels). Error bars are the standard deviation of 8 friction scans at the same location.

above what could be expected from the hydrodynamic no-slip boundary condition, due to the existence of a depletion layer that reduces friction on the carbon wall. By definition, the slip length is given by $b = \eta/f_{SL}$, where f_{SL} is the graphene-liquid friction coefficient. In equilibrium $(t \to \infty)$, f_{SL} is directly proportional to the fluid density in contact with the wall, a structure factor that reflects the liquid-solid commensurability and the fluid-solid (interfacial) energy.2 This relation represents a true thermodynamic equilibrium, which might not be achieved in experiments if the flow is fast. The interfacial energy includes the contribution of van der Waals (vdW) interactions. Our measurements of the electrical double layer reveal a small surface charge of graphene (Figure S4 and text in the SI), which can contribute to the solid-liquid friction coefficient of the ionic liquids.²¹ Since the estimated electrical contribution is negligible for the investigated ionic liquids (<3%, Table S1), we consider only the contribution of van der Waals interactions to f_{SL} as a first approximation. Note, however, that the theory²¹ was not tested on highly concentrated electrolytes like ionic liquids, and hence, deviations are possible. By calculating the Hamaker constant for self-interaction of each component and using mixing rules for Hamaker constants,²⁷ the interaction energy due to vdW

interactions ($W_{\rm vdW}$) can be obtained for each Gr/substrate–liquid system; calculations and assumed parameters are shown in Table S4 and the text in the SI. Figure 2D shows the slip length as a function of $-W_{\rm vdW}$; i.e., a larger/more positive number on the x-axis indicates a stronger interaction. Overall, a larger slip length results from weaker interactions between the liquid and surface. However, the interaction energy on its own does not fully predict the slip length. There is also no relation between the slip length and the viscosity or density of the liquid (Figure S5). Although some experimental works have shown a dependence between slip length and viscosity, theory shows that the influence of the viscosity drops out, and hence, the lack of correlation between viscosities and slip length shown in our results is not surprising.

Figure 2D shows that there is an obvious clustering of the slip length corresponding to ionic liquids and nonionic liquids. One key characteristic of ionic liquids is their interfacial ordering or molecular layering. Molecular layering can be resolved in measurements of the structural force with an AFM tip (see the Methods section). Figure 3A,B reveals the prominent interfacial structure of EMIM FAP on graphene (Gr/Cu and Gr/Si shown) measured over areas of 100 nm × 100 nm. A pronounced interfacial structure was also measured

for EMIM TFSI on graphene (Figure 3C,D), and similar results have been reported for other imidazolium ionic liquids by others on graphene or graphite. For the silicone oil (Figure 3E), there were clear layers close to the surface of graphene, also indicating the arrangement of the molecules on the surface. A weak ordering was revealed for ethylene glycol (Figure S6), while interfacial layering was not resolved for the sucrose solution on Gr/Cu (not shown) and only very rarely on Gr/Si (see Figure 3F). We note that these measurements were taken in maps covering an area across the surface, at multiple locations. Similar out-of-plane structures were observed at all measurement locations, indicating the homogeneity of the in-plane configuration of these systems.

Interfacial layering results from the geometric constraint provided by a smooth surface on molecules of the same size; thus, having a mixture of water and sucrose molecules often disturbs the molecular order. The more prominent interfacial structure in ionic liquids is due to strong ion-ion correlations that are absent in the other liquids. 32 The observed correlation between interfacial ordering and slip is consistent with the finding by molecular dynamic simulations that a significant decrease in interfacial friction stems from such a layered structure.²⁶ As shown in the simulations, these layers influence each other and build stable domains of parallel aligned "blocks" that impact the structure factor at the interface and thus decrease the liquid/graphene commensurability. Based on this, we propose that the different slip length of the investigated liquids reflects not only the different solid-liquid interaction but also the interfacial ordering of the liquids.

Slip Length Dependence on Substrate Underneath Graphene. Figure 2B shows the slip length for the 60 wt % sucrose solution and EMIM FAP in contact with Gr/Cu, Gr/ Au, and Gr/Si at an approach velocity of 6 μ m/s; results for other velocities are shown in Figure S1B in the SI. Here, we varied graphene's doping level by changing the substrate underlying graphene: 13 n-doping on Cu, p-doping on Au, and weak p-doping on SiO₂, 33 which alters the wettability of graphene due to doping-induced modulation of the charge carrier density of graphene and dispersion (attractive) forces between liquid molecules and graphene. 13 Figure 2B shows that the slip length for EMIM FAP is sensitive to the substrate, and the smallest values are obtained on Gr/Si. In the case of sucrose solution, the slip length is largest on Gr/Si, and hence, we observe a reverse influence of the substrates on the slip length, van der Waals interactions cannot predict the subtle variation of the slip length in response to the substrate underneath graphene (Figure 2D). However, the increase of the slip length reflects the increase of the contact angle for each of the liquids (Figure 2C, see dashed lines).

Transition State Theory and Friction-Force Measurements. In the spirit of Eyring's transition state theory, we consider the slip at the solid-liquid interface as a thermally activated rate process facilitated by the shear force. Eyring developed a mathematical model for activated processes, which was adapted later to describe the viscosity of liquids. The model considers that the motion of a molecule is restricted by the barriers due to its neighbors yielding an activation energy (E_a) , and these are overcome by the applied shear stress and the random thermal fluctuations, while the height of the barrier increases with applied pressure. For this process to happen on a surface, vacancies or defects must exist, which occur due to diffusion of the liquid molecules from the surface to the bulk. The average time for the molecule to pass across the barrier

(the rate of hopping, ν') is the Boltzmann factor multiplied by the effective vibration frequency of the molecule ν_0 , *i.e.*

$$\nu' = \nu_0 \exp(-(E_a + P\Omega - \tau \phi)/kT)$$

where τ is the shear stress applied on the molecule and ϕ the shear activation volume (the corresponding length λ along the slip direction is shown in Figure 4A). Ω is the pressure activation volume; the physical interpretation of this parameter is still debated and, hence, is not discussed here, but it is necessary to unambiguously determine $E_{\rm a}$. If we consider a periodic series of these barriers separated by a distance a and allow transitions in both directions, the slip velocity $V_{\rm s}$ is thus the rate of hopping multiplied by the number of vacancies and the length of the hop (distance between barriers) a

$$V_{\rm s} = 2\nu_0 a \, \exp(-(E_{\rm a} + P\Omega)/kT) \, \sinh(\tau \phi/kT) \tag{4a}$$

This simplifies to

$$V_{s} = \vartheta_{0} \exp(-(E_{a} + P\Omega - \tau \phi)/kT) \tag{4b}$$

with $\nu_0 a = \vartheta_0$, and $\tau \phi/kT \gg 1$. The lattice constant of graphene is 2.46 Å, which is taken here as a, and the vibrational frequency of the liquid molecules ν_0 is taken in the range $10^{11}-10^{15}~{\rm s}^{-1}$; e.g., the interionic vibrational frequency of ionic liquids can be as small as $\sim 6 \times 10^{11}~{\rm s}^{-1}$, and for water, the vibrational (librational) frequency is $\sim 2 \times 10^{13}~{\rm s}^{-1}$.

Pioneering simulations have demonstrated that this rate process, and specifically V_s , determines the slip length of the confined fluid molecules between two plates upon shear; those simulations ignored the influence of τ . Here, we assume that the slip of the seven liquids on graphene is a thermally activated process and that it can be promoted by the applied shear. Because hydrodynamic-force measurements cannot be easily modeled due to the varying shear stress and pressure during the approach of the sphere, we determine the characteristics of the rate process, E_a , Ω , and ϕ in friction-force measurements.

We chose two liquids, 60 wt % aqueous sucrose and EMIM FAP, to perform friction measurements on Gr/Au, Gr/Cu, and Gr/Si. To measure friction, a sharp AFM tip was approached to the surface in liquid and slid back and forth over a small (100 nm) line at varying loads and sliding speeds $V_{\rm L}$ (see the Methods section). The measured lateral force represents the force required for the tip to slide while a thin film of liquid molecules remains trapped between the smooth surface and the tip, a phenomenon called hydration lubrication. At least three measurements per substrate and liquid were carried out, and at least two different substrates of each kind were investigated to verify the reproducibility of the data. Figure 4D–I illustrates the influence of both the substrate underneath graphene and the liquid on friction.

In the sliding experiments with the AFM tip, we do not observe the velocity of the rate-controlling process V_s but the sliding velocity V_L . Hence, the friction force F_L is given by ⁴⁰

$$F_{\rm L} = A \frac{E_{\rm a} + P\Omega}{\phi} + A \frac{k_{\rm B}T}{\phi} \ln(V_{\rm L}/V_0)$$
(5)

where V_0 is a reference velocity beyond which the thermal activation process vanishes, and A is the contact area between the tip and graphene.

The dashed lines represent the fits of eq 5 to the experimental results in Figure 4D–I. The logarithmic dependence of friction on $V_{\rm L}$ shown in Figure 4D–I supports the

validity of this model. We determined $V_0 = 40 \text{ m/s}$ for water in temperature-dependent friction-force measurements⁴¹ and assume V_0 to be of the same order of magnitude for the sucrose solution. For the ionic liquid, the interionic vibrational frequency is smaller than that of water, so we reduced V_0 to 0.4 m/s. The fits to the experimental results provide ϕ , E_a , and Ω . According to the model, friction increases with an increase of E_a and Ω and a decrease of the shear activation volume ϕ . E_a Ω , and ϕ relate to the lateral motion of liquid molecules along the graphene surface from the perspective of the transition state theory. Figure 4B,C shows that the thermal activation energy and the shear-activation volume E_a and ϕ are sensitive to the substrate underneath graphene and to the liquid. Here, it is proposed that they provide a molecular lens through which to understand the slip characteristics of the liquids and the influence of the substrate underneath graphene.

MD simulations by Martini *et al.*⁴² have introduced two types of slip at the molecular scale. At low shear forces, individual atoms hop through the energy landscape along the surface from one equilibrium position to another according to Arrhenius dynamics: a phenomenon called defect slip and described *via* a simplified Eyring's transition state theory. High shear forces lead to a transition to global slip, where the transition state vanishes, and the molecules move in a collective fashion, all molecules slipping downstream at the same speed. The stress conditions in our measurements are consistent with the molecular mechanism of defect slip introduced in ref 42, which supports the application of the transition state theory.

Our conceptual framework for slip on smooth graphene is thus based on transition state theory. In Vinogradova's model, the slip length is given as $V_s/\dot{\gamma}_s$. For a given approach velocity V and surface separation, D, $\dot{\gamma}_s = V/D$ is the same for all the liquids, and hence, the slip length should be proportional to the slip velocity $b \propto V_s = \vartheta_0 \exp(-(E_a + P\Omega - \tau\phi)/kT)$, where ϑ_0 is a constant for each liquid. The pressure and the shear stress change upon the approach of the colloid to the surface and along the radial direction, meaning that a quantitative comparison is not possible. We thus compare in Figure 5A the experimentally measured slip length with the calculated value of V_s/ϑ_0 at the radial position of the maximum shear rate at the graphene surface, $r_0 = (2RD/3)^{1/2}$; ¹⁶ several D-values are taken to test this relation at r_0 .

The inset in Figure 5A shows that the measured slip length decreases roughly exponentially with E_a for the two liquids. This is due to the small magnitude and negligible effect of the applied work by the shear force $(\tau_0 \phi)$ at r_0 and the pressure $(P_0\Omega \text{ at } r_0)$ in the hydrodynamic-force measurements, so that the activation energy plays the key role in dictating slip. This can be understood as a variation of the energy landscape of the graphene/liquid interface and of the transition state of the liquid molecules induced by the substrate underneath graphene for each liquid. The metal substrates inducing a higher degree of doping have thus a prominent influence on the slip velocity, but the polarity of doping (p- or n-type) seems to be less relevant. Strikingly, the influence of the doping on the activation energy is very different for the two investigated liquids; assuming Gr/Si as a "reference" activation energy due to its weak doping, the activation energy significantly increases for the ionic liquid on Gr/Au and further on Gr/Cu, whereas it decreases for the sucrose solution, more on Gr/Cu compared to Gr/Au. It is known that graphene interacts with charged and uncharged molecules in

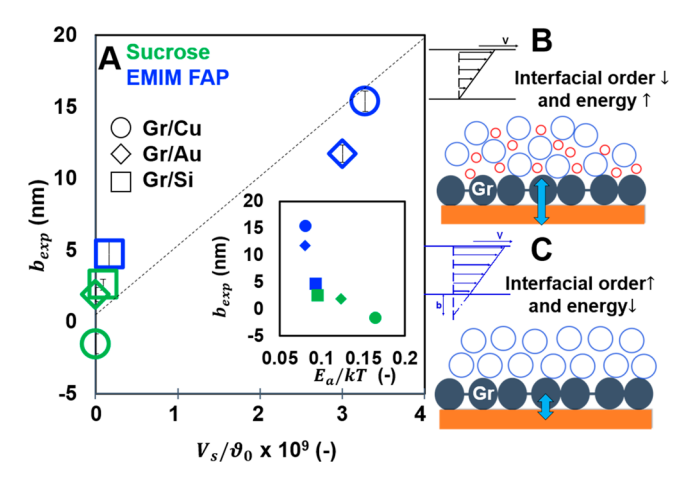


Figure 5. Relation between slip, interfacial order, and transition state theory. (A) Comparison between the measured slip length in hydrodynamic-force measurements for sucrose solution and EMIM FAP on the three substrates, and an estimated slip (dotted line) based on the transition state theory, using the parameters determined in friction-force measurements (E_a , ϕ , and Ω). The inset shows the estimated activation energy E_a , which is the parameter that dominates the slip under the stress conditions of the hydrodynamic-force measurements. Slip length values are the average of ~ 10 measurements at 6 μ m/s, and error bars are the standard deviation. (B, C) Cartoon of the proposed mechanism dictating slip along graphene: the order/disorder of the liquid as well as the solid-liquid interaction energy, both factors influencing the activation energy E_a . (B) Representation of a liquid that does not exhibit prominent interfacial layering, e.g., the sucrose solution (a mixture of molecules of different size) and is characterized by high solid-liquid interaction energy; (C) representation of a molecular liquid that forms well-ordered layers at the interface with graphene and is characterized by moderately weak solid-liquid interactions.

its close vicinity via the delocalized π -electrons, and hence, molecular adsorption is sensitive to graphene doping. A3,44 The adsorption strength of the liquid molecules to the surface affects the depletion layer and thereby contributes to the friction coefficient and the slip process. Although we do not have a clear explanation for this different behavior yet, our results suggest that n- and p-doping effects on the slip of uncharged (sucrose/water) and charged and strongly correlated molecules (IL anions and cations) could be significantly different.

Experiments and simulations estimate slip lengths for water in carbon nanotubes (CNTs) of sub-10 nm diameter from about 1 up to 1400 nm. 45,46 Simulations and theoretical works 24 have proposed that the slip length is a very sensitive probe of water depletion at carbonaceous surfaces with contact angles between 40° and 150°, with $b\sim\delta^4$ (δ is the depletion layer thickness). This depletion layer is most often justified by the small liquid—graphene (van der Waals) interaction energy and thereby by the low interfacial friction coefficient. This explains why the static contact angle is typically used as a representative of the influence of the solid—liquid interfacial energy on slip of water on surfaces of different wettabilities. Despite this, we reinforce that the commonly reported relationship for pure water 24 is inadequate for our systems with polar, nonpolar, and ionic liquids on graphene supported by different substrates (Figure 2C,D).

Simulations also clarify that the liquid/solid friction coefficient depends not only on the solid—liquid interactions

but also on the interfacial structure of the liquid, the smoothness of the surface, and the resulting incommensurability between the liquid and the solid surface. 11 The curvature-related incommensurability between water and the inner surface of CNTs leads to a decrease of the structure factor and thereby to a relevant decrease of the friction coefficient, which, indeed, explains the ultrafast flow of water. It is also shown that the prominent interfacial layering of decane and ethanol at the interface with flat graphene is responsible for the significant slip. 26 This suggests that the molecular layering resolved for the ionic liquids and the silicone oil at the graphene/liquid interface is related to their greater slip lengths compared to the sucrose solution and even ethylene glycol. According to the proposed model, the activation energy quantifies the various influencing factors on the friction coefficient.

We emphasize that the behavior of sucrose solutions and pure water may be different, and hence, our results do not contradict the reported ultrafast slip of water along graphene. In fact, our previous work demonstrated the prominent molecular layering of water and of NaCl and KCl solution on Gr/Si, which supports the larger slip length for water compared to sucrose solutions. Furthermore, the activation energy is similar to that estimated for EMIM FAP (23 kT for water and 20 kT for 10 mM NaCl on Gr/Si compared to 23 kT for EMIM FAP), while the shear activation volume is much larger (2–4 nm³ for water vs 0.7 nm³ for the ionic liquid), both supporting a large slip length of the water molecules along the graphene interface.

CONCLUSIONS

In summary, measurements across liquids with varied properties support the relevance of interfacial ordering in determining slip characteristics. This suggests that liquid structure, like interfacial layers, promotes slip, and this phenomenon appears to be as relevant as the solid-liquid interaction energy. We have also shown that the slip boundary condition along the graphene plane of two liquids, an ionic liquid with a high charge density and an aqueous solution with sucrose, is sensitive to the substrate underneath graphene. Our model describes the slip behavior via a transition state theory and quantifies the effect of the substrate underneath graphene via the thermal activation energy for slip. Much higher shear forces than those applied in our experiments could lead to a vanishing transition state and a different slip behavior. Since interfacial slip can have prominent consequences on the pressure drop, on electrical and diffusive transport through nanochannels, and on friction, this work is expected to be relevant to many applications. In particular, systems incorporating both induced shear and nanoconfinement (such as liquid phase sensors or membranes) will need to be designed with slip in mind as they see increased use. Furthermore, it may be possible to actively tune the slip behavior as the doping of graphene can be dynamically modulated via electrical bias. We also note that environmental effects (i.e., substrate effects) are likely not only observed to be influential for graphene but also important to all 2D materials (and therefore their slip properties), but the extent and importance of the effect will need to be verified.

METHODS

Materials. Seven liquids were investigated: aqueous sucrose 60 wt % solution (sucrose from MP Biomedical and Millipore Milli-Q ultrapurified water), ethylene glycol (Fisher Scientific), silicone oil

(100 cSt, Sigma-Aldrich, Inc.), 1-ethyl-3-methylimidazolium tris-(pentafluoroethyl)trifluorophosphate (abbreviated EMIM FAP, Merck kGaA, ≥98% purity), 1-ethyl-3-methylimidazolium bis-(trifluoromethylsulfonyl)imide (EMIM TFSI, Iolitec Ionic Liquid Technologies GmbH, 99% purity), 1-butyl-3-methylimidazolium bis(trifluoromethylsulfonyl)imide (BMIM TFSI, Iolitec Ionic Liquid Technologies GmbH, 99% purity), and 1-hexyl-3-methylimidazolium bis(trifluormethylsulfonyl)imide (HMIM TFSI, Iolitec Ionic Liquid Technologies GmbH, 99% purity). Liquid properties are shown in Table S1.

The liquids (except silicone oil, EMIM FAP, HMIM TFSI, and BMIM TFSI due to their higher viscosities) were filtered using a 0.2 μm PTFE filter. The ethylene glycol and silicone oil were stored under standard conditions and used as received from the supplier. Sucrose solutions were prepared to be 60% sucrose by weight (wt %), using ultrapure water purified by a Millipore Milli-Q purification system. The solution was stored under refrigeration before use, with a stirring/temperature equilibration period immediately before each use. All ionic liquids were stored in a vacuum desiccator, with small quantities taken out and dried before measurement in a vacuum oven at 50 °C for 24+ hours.

Viscosities for all liquids were taken from the literature (see references in Table S1). Since viscosity can change with temperature, and our AFM system does not have *in situ* temperature monitoring, the assumed values may have some error. However, the solution temperature immediately before and after completion of an experiment was consistently measured to be between 25 and 26 °C. The reported viscosity at 25 °C produced generally good fits to the measured data.

Graphene Synthesis, Transfer, and Characterization. Monolayer graphene was synthesized by low-pressure chemical vapor deposition (CVD). A 25 µm thick Cu foil (MTI Corporation, Richmond, CA) was cleaned by soaking in acetic acid (Fisher Scientific) and a deionized (DI) water bath and rinsing with acetone and isopropyl alcohol. The air-dried Cu foil was then placed on a quartz boat and put inside of a CVD tube furnace (Rocky Mountain Vacuum Tech, Inc., Aurora, CO). The detailed CVD synthesis is described in an earlier report. 48 Briefly, the Cu foil was first annealed at 1050 °C for 30 min with flowing H2 gas. Then, graphene was grown by flowing CH₄ and H₂ for 2 min at 1050 °C, followed by cooling under an Ar atmosphere. Poly(methyl methacrylate) (PMMA) (950A2, MicroChem, Westborough, MA) was spin-coated on as-grown graphene at 6000 rpm for 30 s and baked on a hot plate at 110 °C for 2 min, while graphene on the backside of the Cu foil was removed by oxygen plasma (pressure = 150 mTorr, power = 500 W, time = 5 s) (Diener GmbH). We etched out Cu foil by floating PMMA/Gr/Cu on the copper etchant (sodium persulfate solution (Sigma-Aldrich, St. Louis, MO)) and transferred PMMA/Gr on a DI water bath several times to remove residual ions on the graphene surface. Afterward, PMMA/Gr was transferred to target substrates, dried in ambient conditions, and finally immersed in an acetone bath to remove the PMMA layer. Thermal annealing of graphene on various substrates was performed at 400-450 °C for 3-7 h under an Ar/H₂ atmosphere to eliminate residual polymers⁴⁹ and bubbles and water trapped between the graphene layer and the substrate.

Three different types of substrates (SiO₂, Au, Cu) were prepared in this study. Metallic substrates were prepared by depositing 100 nm Au/3 nm Cr or 200 nm Cu on a 300 nm thick thermal oxide Si wafer (UniversityWafer, South Boston, MA) using a thermal evaporator (Nano36, Kurt J. Lesker, Jefferson Hills, PA) or e-beam evaporator (FC-2000, Temescal, Livermore, CA), respectively. Raman spectroscopy (Nanophoton Raman 11) was performed on the annealed graphene on different substrates with 532 nm excitation.

The RMS roughness as determined by AFM imaging (Cypher, Asylum Research, Goleta, CA) was found to be less than 3 nm for all samples, and care was taken to restrict measurements to areas with a roughness smaller than ~ 1.8 nm. If the slip length is smaller than the combined (contact) roughness (< 3 nm), this indicates no slip.

Contamination and Reproducibility. While special care was taking during fabrication to produce clean, uncontaminated graphene

using standard methods like annealing, it has been reported that ambient hydrocarbons may preferentially adsorb to graphene surfaces exposed to air so and alter its surface properties. Hydrocarbon adsorption may happen within 10s of minutes of exposure to air, and some adsorbates can remain even after annealing, particularly compounds containing aromatic rings that can match graphene's lattice structure. In the present study, we attempted to mitigate ambient contamination by storing all samples in a vacuum desiccator after postfabrication and annealing, or after opening the vacuumsealed shipping packaging in the case of graphene used as-grown on copper foil. Samples were kept under vacuum until immediately before measurement and were immersed in the liquid of interest immediately after removal from the desiccator. Even strictly adhering to these precautions, hydrocarbon contamination is still possible. Furthermore, adsorption of waterborne contaminants on graphene is also possible. 51 Thus, all measurements were replicated at more than one location on a given sample, and measurements were repeated across different samples to ensure reproducibility of the measurements. We found good agreement between samples prepared at different times, prepared using different methods, and stored in the vacuum desiccator for different lengths of time, indicating that contamination did not play a major role in influencing the results.

Colloidal Probe Preparation. Monodisperse silica microspheres (20 µm diameter, microParticles GmbH) were used for the hydrodynamic-force measurements. Spheres of this size were found to strike a reasonable balance between surface quality (roughness/ uniformity) and a diameter of the correct size to measure forces within the sensitivity of our AFM across a range of viscosities. The microspheres were stored in DI solution until preparation and then transferred to freshly cleaved mica in droplet form. While waiting for the droplet to evaporate, the spring constants of the tipless cantilevers (k) were determined using the thermal calibration method.⁵² Using an optical microscope, a micromanipulator, and an etched tungsten wire, a small amount of epoxy (J-B Weld Steel Reinforced Epoxy, J-B Weld Company) was placed at the end of each cantilever. A separate etched tungsten wire was used immediately afterward to pick up individual microspheres and place them on top of the epoxy. The system was then left to set for at least 24 h before use.

While surface imperfections are noticeable on some spheres using an optical microscope, the surface quality and sphere size cannot be accurately determined until after gluing is complete. These were quantified using both scanning electron microscopy (SEM) and inverted imaging using an AFM. ⁵³ We found that spheres can vary widely in terms of roughness and imperfections, while diameters are more consistent but still vary slightly. To help mitigate these issues and simplify the comparison across systems, we used the same sphere for all hydrodynamic-force measurements. Both imaging methods gave a sphere radius of \sim 8.9 μ m, and inverted imaging gave a roughness of 322.8 pm for a $100 \times 100 \text{ nm}^2$ area close to the contact.

Hydrodynamic-Force Measurements and Analysis. The JPK Nanowizard atomic force microscope (Bruker Nano GmbH, JPK BioAFM) located in an acoustic chamber was used throughout this study. For the sucrose solution, ethylene glycol, and silicone oil, the samples were fixed in a homemade fluid-cell with 2 mL of solution, with the cell covered by a membrane to minimize evaporation. The IL measurements were performed in a ~0.2 mL droplet of IL in a sealed cell with an ultra-high-purity dry nitrogen atmosphere. All systems were equilibrated for at least 1 h before the measurements started. Hydrodynamic-force measurements used a tipless cantilever with spring constant $k \sim 0.334$ N/m (Mikromasch USA, HQ:CSC37/ tipless). Silica microspheres were glued to the tipless cantilevers using a micromanipulator, as described above. Prior to the force measurements, several 25 μm imes 25 μm regions were imaged in contact mode after equilibration to ensure that measurements were performed far away from defects and boundaries.

Hydrodynamic-force measurements were carried out by quickly driving the as-prepared colloid probe toward the investigated surface. The approach started from a distance as far from the surface as permitted in our AFM system (\sim 6.5 μ m), with data being collected for \sim 3 μ m from the surface. Most AFM systems exhibit a virtual

deflection resulting from instrumental errors; this is usually accounted for by assuming that some range far from the surface is influenced only by this virtual deflection, fitting a linear equation to the range, and subtracting the result from the entire curve. This approach is complicated in our measurements where the tip experiences an acceleration very far from the surface (see Figure S7), while it is influenced non-negligibly by the hydrodynamic force at closer distances. We attempted to account for the virtual deflection using the slope at multiple surface separations between \sim 1.4 and 2.8 μ m and found that, with our analysis approach, described later, there is a negligible difference in the resulting slip length.

Another key aspect for the reliable determination of the slip length is the proper determination of the cantilever sensitivity (the deflection in nm per volts on the photodetector). This has been described in detail in ref 14. Briefly, a large sphere in contact with a hard surface slides slightly while it is pressed on the surface. The small friction force contributes to the normal deflection and causes a hysteresis between approach and retraction. As a result, the apparent hard wall differs between approach and retraction during the calibration of the cantilever sensitivity—neither gives the true sensitivity, with the real value being approximately the average of the two. Using the average, though, does not give the true contact point either in the approach or in the retraction. For the analysis of the slip length, we used the individual sensitivity value, resulting in a precise determination of the contact point and of the surface separation. Adjusting the sensitivity to the single value, however, changes the distance at which a force seemingly occurs, affecting the force profile itself. We found that the effect of the sensitivity (average vs single value) on the slip length is similar to the standard deviation of the measurements, with both giving good quality fits, and hence, it is an acceptable approach (Figure S8).

The force balance during the approach of the cantilever to the surface is given by

$$F_{\rm b}(t) + F_{\rm b}(t) + F_{\rm d}(t) + F_{\rm c}(t) = 0$$

where F_h is the hydrodynamic force, F_k the measured spring force (F_k = $k \cdot x$, x being the normal deflection), F_d the viscous drag of the cantilever, and F_s the total surface force. The latter results from van der Waals, electrostatic (for the ionic liquids and aqueous solutions), and solvation forces and is only relevant at separations $D \lesssim 30$ nm. The force balance was solved at separations larger than 30 nm, where the surface force is zero to a good approximation $(F_s \sim 0)$. Furthermore, $R \gg D$, which allows applying Reynold's lubrication theory (eqs 2 and 3) to calculate the hydrodynamic force $F_{\rm h}$, i.e., to eliminate the effect of higher-order terms at larger separations as described by Brenner's model. 18,25 To determine the hydrodynamic force, the instantaneous velocity of the colloid \dot{D} was used, which differs from the piezo velocity. At surface separations smaller than ~30 nm, the hydrodynamic force suggested an increase in slip length; i.e., the hydrodynamic force F_h was smaller than predicted with the fitted slip length.

Following the approach developed by Neto's group to determine the slip length, ¹⁸ we modeled the drag force as a function of the piezo driving velocity V and an effective drag length of the cantilever $L_{\rm e}$ according to $F_{\rm d}=-6\pi\eta L_{\rm e}V$. The separation between colloid and surface is D=x+z, z being the piezo position and x the deflection of the cantilever. The corresponding instantaneous velocity is $\dot{D}=\dot{x}+\dot{z}$. Solving the force balance for the deflection of the cantilever x' at the time step $t'=t+\Delta t$ gives

$$x' = -\frac{6\pi\eta R^{2}(\dot{z} + \dot{x}')}{k(x' + z')} f * \left(\frac{D'}{b}\right) - \frac{6\pi\eta L_{e}\dot{z}}{k}$$

with the cantilever velocity (\dot{x}') and the separation D' calculated still at t. The separation between colloid and substrate surface is then actualized at $t+\Delta t$ with x' and z', and the slip function f^* is then determined at $t+\Delta t$, as well. The cantilever velocity can then be calculated at $t+\Delta t$ as

$$\dot{x}' = -\frac{-x - \frac{\Delta t}{2}\dot{x} - \frac{6\pi\eta R^2z}{k(x'+z')}f^*\left(\frac{D'}{b}\right) - \frac{6\pi\eta L_c\dot{z}}{k}}{\frac{\Delta t}{2} + \frac{6\pi\eta R^2}{k(x'+z')}f^*\left(\frac{D'}{b}\right)}$$

which enables the calculation of \dot{D} and the hydrodynamic force using eq 2 and the spring force. Because the magnitude of F_d is small and remains constant with separation, it affects only the spring force at large separations where F_{hyd} is still negligible, while F_{hyd} increases as the colloid is closer to the surface. This disentanglement of the two forces enables us to determine $L_{\rm e} \sim 90~\mu{\rm m}$ for the investigated cantilever type. The system of equations has only one unknown parameter, b, that is determined by minimizing the sum of the residuals squared when comparing the calculated and measured spring force at each time step. The range of D between 30 nm and 1.4 μm was ultimately chosen for the fit of the model to the experimental results. We noticed that, as the velocity of approach V increased to 10 and 20 μ m, the deviation of the model from the experimental results became often more significant (\$75 nm). We do not have an explanation for these trends yet. We also performed control measurements of the slip length on silica surfaces for the sucrose solution using stiffer cantilevers (spring constant = 1.108 N/m), and the slip lengths were in good agreement with those reported here, which gives us confidence that our results are reliable in the selected range of approach velocities.

A final aspect to account for is the chemical asymmetry of the systems since a silica sphere approaches a graphene surface, and the slip boundary condition may be different on each surface. Equation 3 assumes chemical symmetry, *i.e.*, that the two surfaces have the same slip boundary condition. It is, however, common practice to use eq 3 to determine an average slip length b in asymmetric systems, 23,25,54 and hence, we have followed this approach in the paper. In addition to this, we carried out reference measurements on a cleaned, naturally oxidized silicon wafer in the 7 liquids using the same silica probe, representing a chemically symmetric system. These results allow us to find the slip lengths of the liquids on a silica surface (b_2) . With the value of b_2 , we used the approach described in ref 19 to estimate the slip length along graphene (b_1) . Here, the computed f^* with the average b according to eq 3 is equated to the following expression for asymmetric systems:

$$f^* = -\frac{2AD}{BC} - \frac{2D}{C - B} \left(\frac{(B + D)(B - A)}{B^2} \ln \left(1 + \frac{B}{D} \right) - \frac{(C + D)(C - A)}{C^2} \ln \left(1 + \frac{C}{D} \right) \right)$$

where $A = b_1(2 + k)$, $B = 2b_1(2 + k + (1 + k + k^2)^{0.5})$, $C = 2b_1(2 + k - (1 + k + k^2)^{0.5})$, and $k = b_2/b_1 - 1$. In this way, b_1 can be determined for each liquid (Figure S3).

Friction-Force Measurements. Friction-force measurements used sharp-tip cantilevers with normal spring constants $k \sim 0.3-0.5$ N/m (Mikromasch USA, HQ:CSC37). The lateral sensitivities were determined in each liquid based on the method described in ref 55. Friction-force measurements were performed by repeatedly sliding a sharp AFM tip across a 100 nm line (~8 traces and retraces for a single data point) on the graphene surface, measuring the lateral force acting on the tip during the process; the friction force is given as the half of the difference between trace and retrace lateral forces. A new tip was used for each experiment since we have observed that results become less reliable as the tip becomes blunted. The tips used in the experiments shown here have a radius R of \sim 97 \pm 2 nm, as determined by scanning electron microscopy imaging. The reproducibility of the experiments was confirmed by replica experiments with different tips. Considering that the drift of our instrument is ~2 nm per 1 h and that the slowest scan takes \sim 1 s (2 s for trace and retrace), the drift can be considered to have a negligible effect, and so the tip slides along the same line. The small error bars that give the friction force averaged over ~8 friction loops support that the properties of graphene do not gradually change during the sliding process.

Normal-Force Measurements. Normal-force measurements were performed with AFM cantilevers with $k \sim 0.45-0.7$ N/m with sharp tips (R=20 nm) as well as silica colloids ($R=2.5~\mu m$) glued to tipless cantilevers. The sharp tip was used to measure the short-range structural forces in the seven liquids on Gr/Cu and Gr/Si, whereas the colloid is more sensitive to long-range surface forces and was used to obtain information about the electrical double layer in aqueous solutions. The same procedures were followed to calibrate the tips as described earlier.

After 1 h of equilibration in each liquid at 25 °C, normal forces were measured. Prior to the force measurements, several regions were imaged in contact mode after equilibration in liquid to select relatively large areas (\sim 5 μ m \times 5 μ m) far away from defects and boundaries. Force—separation curves were collected at an approach speed of 20 nm s⁻¹.

Contact Angle Measurements. Contact angles were measured using a Ramé-Hart Model 250 contact angle goniometer. Images of the measurements and their contact angles are shown in Figure S2. Samples and liquids were carried in a vacuum desiccator to a separate building where the goniometer was located. Samples were placed on the goniometer stage after leveling the stage and calibrating the pixel size. The camera was then focused on the front edge of the sample, and a $\sim\!10~\mu\mathrm{L}$ drop of liquid was manually placed on the surface using a micropipette. The goniometer software was used to capture the images and calculate the contact angles. Each reported contact angle is the average of 10 measurements taken over 10 s, and the uncertainty is the standard deviation of those measurements.

ASSOCIATED CONTENT

Supporting Information

The Supporting Information is available free of charge at https://pubs.acs.org/doi/10.1021/acsnano.1c01884.

Calculation of van der Waals interactions, description of long-range surface forces, discussion of the electrical contributions to the friction coefficient, tables of liquid properties and collected slip lengths, and figures showing slip lengths not shown in the main text, contact angles, results of the asymmetric slip analysis, force—distance curves, correlation of slip length to liquid properties, structural forces not show in the main text, motion of the tip during approach, and the effects of using the measured vs average cantilever sensitivity (PDF)

AUTHOR INFORMATION

Corresponding Authors

SungWoo Nam — Department of Materials Science and Engineering, University of Illinois at Urbana—Champaign, Urbana, Illinois 61801, United States; Department of Mechanical Science and Engineering, University of Illinois at Urbana—Champaign, Urbana, Illinois 61801, United States; orcid.org/0000-0002-9719-7203; Phone: +1 217 300 0267; Email: swnam@illinois.edu

Rosa M. Espinosa-Marzal — Department of Civil and Environmental Engineering, University of Illinois at Urbana—Champaign, Urbana, Illinois 61801, United States; Department of Materials Science and Engineering, University of Illinois at Urbana—Champaign, Urbana, Illinois 61801, United States; orcid.org/0000-0003-3442-2511; Phone: +1 217 607 3856; Email: rosae@illinois.edu

Authors

Gus Greenwood — Department of Civil and Environmental Engineering, University of Illinois at Urbana—Champaign, Urbana, Illinois 61801, United States

- Jin Myung Kim Department of Materials Science and Engineering, University of Illinois at Urbana–Champaign, Urbana, Illinois 61801, United States
- Qianlu Zheng Department of Civil and Environmental Engineering, University of Illinois at Urbana—Champaign, Urbana, Illinois 61801, United States
- Shahriar Muhammad Nahid Department of Mechanical Science and Engineering, University of Illinois at Urbana—Champaign, Urbana, Illinois 61801, United States

Complete contact information is available at: https://pubs.acs.org/10.1021/acsnano.1c01884

Notes

The authors declare no competing financial interest.

ACKNOWLEDGMENTS

We thank A. Martini and S. Lichter for fruitful discussions about the relation between slip length and the transition state theory. This research was carried out in part in the Materials Research Laboratory Central Research Facilities, University of Illinois. This material is based upon work supported by the National Science Foundation under Grant NSF CMMI-1904216 and under Grant NSF CBET-1916609.

REFERENCES

- (1) Vinogradova, O. I. Drainage of a Thin Liquid Film Confined between Hydrophobic Surfaces. *Langmuir* 1995, 11, 2213–2220.
- (2) Bocquet, L.; Charlaix, E. Nanofluidics, from Bulk to Interfaces. Chem. Soc. Rev. 2010, 39, 1073–95.
- (3) Majumder, M.; Chopra, N.; Andrews, R.; Hinds, B. J. Nanoscale Hydrodynamics: Enhanced Flow in Carbon Nanotubes. *Nature* **2005**, 438, 44.
- (4) Geim, A. K.; Novoselov, K. S. The Rise of Graphene. *Nat. Mater.* **2007**, *6*, 183–91.
- (5) Geim, A. K. Graphene: Status and Prospects. Science 2009, 324, 1530-4
- (6) Snapp, P.; Kim, J. M.; Cho, C.; Leem, J.; Haque, M. F.; Nam, S. Interaction of 2D Materials with Liquids: Wettability, Electrochemical Properties, Friction, and Emerging Directions. *NPG Asia Mater.* **2020**, *12*, 1–16.
- (7) Celebi, A. T.; Barisik, M.; Beskok, A. Surface Charge-Dependent Transport of Water in Graphene Nano-Channels. *Microfluid. Nanofluid.* **2018**, 22, 7.
- (8) Kumar Kannam, S.; Todd, B.; Hansen, J. S.; Daivis, P. J. Slip Length of Water on Graphene: Limitations of Non-Equilibrium Molecular Dynamics Simulations. *J. Chem. Phys.* **2012**, *136*, 024705.
- (9) Radha, B.; Esfandiar, A.; Wang, F. C.; Rooney, A. P.; Gopinadhan, K.; Keerthi, A.; Mishchenko, A.; Janardanan, A.; Blake, P.; Fumagalli, L.; Lozada-Hidalgo, M.; Garaj, S.; Haigh, S. J.; Grigorieva, I. V.; Wu, H. A.; Geim, A. K. Molecular Transport through Capillaries Made with Atomic-Scale Precision. *Nature* 2016, 538, 222–5.
- (10) Suk, M. E.; Aluru, N. R. Molecular and Continuum Hydrodynamics in Graphene Nanopores. *RSC Adv.* **2013**, *3*, 9365–9372
- (11) Falk, K.; Sedlmeier, F.; Joly, L.; Netz, R. R.; Bocquet, L. Molecular Origin of Fast Water Transport in Carbon Nanotube Membranes: Superlubricity *versus* Curvature Dependent Friction. *Nano Lett.* **2010**, *10*, 4067–4073.
- (12) Xie, Q.; Alibakhshi, M. A.; Jiao, S.; Xu, Z.; Hempel, M.; Kong, J.; Park, H. G.; Duan, C. Fast Water Transport in Graphene Nanofluidic Channels. *Nat. Nanotechnol.* **2018**, *13*, 238–245.
- (13) Ashraf, A.; Wu, Y.; Wang, M. C.; Yong, K.; Sun, T.; Jing, Y.; Haasch, R. T.; Aluru, N. R.; Nam, S. Doping-Induced Tunable Wettability and Adhesion of Graphene. *Nano Lett.* **2016**, *16*, 4708–4712.

- (14) Zhu, L.; Attard, P.; Neto, C. Reliable Measurements of Interfacial Slip by Colloid Probe Atomic Force Microscopy. Ii. Hydrodynamic Force Measurements. *Langmuir* **2011**, *27*, 6712–9.
- (15) Zhu, Y.; Granick, S. Limits of the Hydrodynamic No-Slip Boundary Condition. *Phys. Rev. Lett.* **2002**, *88*, 106102.
- (16) Chan, D. Y. C.; Horn, R. G. The Drainage of Thin Liquid-Films between Solid-Surfaces. *J. Chem. Phys.* **1985**, 83, 5311–5324.
- (17) Reynolds, O. Iv. On the Theory of Lubrication and Its Application to Mr. Beauchamp Tower's Experiments, Including an Experimental Determination of the Viscosity of Olive Oil. *Philos. Trans R. Soc.* **1886**, *177*, 157–234.
- (18) Zhu, L.; Attard, P.; Neto, C. Reliable Measurements of Interfacial Slip by Colloid Probe Atomic Force Microscopy. I. Mathematical Modeling. *Langmuir* **2011**, *27*, 6701–11.
- (19) Zhu, L.; Attard, P.; Neto, C. Reconciling Slip Measurements in Symmetric and Asymmetric Systems. *Langmuir* **2012**, 28, 7768–74.
- (20) Zhu, L.; Neto, C.; Attard, P. Reliable Measurements of Interfacial Slip by Colloid Probe Atomic Force Microscopy. III. Shear-Rate-Dependent Slip. *Langmuir* **2012**, *28*, 3465–73.
- (21) Bocquet, L.; Barrat, J. L. Flow Boundary Conditions from Nano- to Micro-Scales. *Soft Matter* **2007**, *3*, 685–693.
- (22) Han, M. W.; Espinosa-Marzal, R. M. Electroviscous Retardation of the Squeeze out of Nanoconfined Ionic Liquids. *J. Phys. Chem. C* **2018**, 122, 21344–21355.
- (23) Honig, C. D.; Ducker, W. A. No-Slip Hydrodynamic Boundary Condition for Hydrophilic Particles. *Phys. Rev. Lett.* **2007**, *98*, 028305.
- (24) Huang, D. M.; Sendner, C.; Horinek, D.; Netz, R. R.; Bocquet, L. Water Slippage *versus* Contact Angle: A Quasiuniversal Relationship. *Phys. Rev. Lett.* **2008**, *101*, 226101.
- (25) Honig, C. D. F.; Ducker, W. A. Thin Film Lubrication for Large Colloidal Particles: Experimental Test of the No-Slip Boundary Condition. *J. Phys. Chem. C* **2007**, *111*, 16300–16312.
- (26) Falk, K.; Sedlmeier, F.; Joly, L.; Netz, R. R.; Bocquet, L. Ultralow Liquid/Solid Friction in Carbon Nanotubes: Comprehensive Theory for Alcohols, Alkanes, Omcts, and Water. *Langmuir* **2012**, 28, 14261–72.
- (27) Israelachvili, J. N. van der Waals Forces between Particles and Surfaces. In *Intermolecular and Surface Forces*; Academic Press: London, 2011; pp 253–289.
- (28) Craig, V. S.; Neto, C.; Williams, D. R. Shear-Dependent Boundary Slip in an Aqueous Newtonian Liquid. *Phys. Rev. Lett.* **2001**, 87, 054504.
- (29) Atkin, R.; Warr, G. G. Structure in Confined Room-Temperature Ionic Liquids. J. Phys. Chem. C 2007, 111, 5162–5168.
- (30) Carstens, T.; Gustus, R.; Hofft, O.; Borisenko, N.; Endres, F.; Li, H.; Wood, R. J.; Page, A. J.; Atkin, R. Combined STM, AFM, and DFT Study of the Highly Ordered Pyrolytic Graphite/1-Octyl-3-Methyl-Imidazolium Bis(trifluoromethylsulfonyl)imide Interface. *J. Phys. Chem. C* 2014, *118*, 10833–10843.
- (31) Jo, S.; Park, S. W.; Shim, Y.; Jung, Y. Effects of Alkyl Chain Length on Interfacial Structure and Differential Capacitance in Graphene Supercapacitors: A Molecular Dynamics Simulation Study. *Electrochim. Acta* **2017**, *247*, 634–645.
- (32) Espinosa-Marzal, R. M.; Han, M.; Arcifa, A.; Spencer, N. D.; Rossi, A. Ionic Liquids at Interfaces and Their Tribological Behavior. In *Encyclopedia of Interfacial Chemistry*; Wandelt, K., Ed.; Elsevier: Oxford, 2018; pp 172–194.
- (33) Giovannetti, G.; Khomyakov, P. A.; Brocks, G.; Karpan, V. M.; van den Brink, J.; Kelly, P. J. Doping Graphene with Metal Contacts. *Phys. Rev. Lett.* **2008**, *101*, 026803.
- (34) Eyring, H. The Activated Complex in Chemical Reactions. *J. Chem. Phys.* **1935**, 3, 107–115.
- (35) Eyring, H. Viscosity, Plasticity, and Diffusion as Examples of Absolute Reaction Rates. *J. Chem. Phys.* **1936**, *4*, 283–291.
- (36) Penna, T. C.; Faria, L. F.; Matos, J. R.; Ribeiro, M. C. Pressure and Temperature Effects on Intermolecular Vibrational Dynamics of Ionic Liquids. *J. Chem. Phys.* **2013**, *138*, 104503.
- (37) Ahmed, M.; Namboodiri, V.; Singh, A. K.; Mondal, J. A. On the Intermolecular Vibrational Coupling, Hydrogen Bonding, and Libra-

- tional Freedom of Water in the Hydration Shell of Mono- and Bivalent Anions. J. Chem. Phys. 2014, 141, 164708.
- (38) Lichter, S.; Martini, A.; Snurr, R. Q.; Wang, Q. Liquid Slip in Nanoscale Channels as a Rate Process. *Phys. Rev. Lett.* **2007**, 98, 226001.
- (39) Ma, L.; Gaisinskaya-Kipnis, A.; Kampf, N.; Klein, J. Origins of Hydration Lubrication. *Nat. Commun.* **2015**, *6*, 6060.
- (40) Briscoe, B.; Evans, D. The Shear Properties of Langmuir-Blodgett Layers. *Proc. R. Soc. London A* **1982**, 380, 389–407.
- (41) Diao, Y.; Greenwood, G.; Wang, M. C.; Nam, S.; Espinosa-Marzal, R. M. Slippery and Sticky Graphene in Water. ACS Nano **2019**, 13, 2072–2082.
- (42) Martini, A.; Roxin, A.; Snurr, R. Q.; Wang, Q.; Lichter, S. Molecular Mechanisms of Liquid Slip. *J. Fluid Mech.* **2008**, 600, 257–269.
- (43) Huttmann, F.; Martinez-Galera, A. J.; Caciuc, V.; Atodiresei, N.; Schumacher, S.; Standop, S.; Hamada, I.; Wehling, T. O.; Blugel, S.; Michely, T. Tuning the van der Waals Interaction of Graphene with Molecules via Doping. *Phys. Rev. Lett.* **2015**, *115*, 236101.
- (44) Schumacher, S.; Wehling, T. O.; Lazic, P.; Runte, S.; Forster, D. F.; Busse, C.; Petrovic, M.; Kralj, M.; Blugel, S.; Atodiresei, N.; Caciuc, V.; Michely, T. The Backside of Graphene: Manipulating Adsorption by Intercalation. *Nano Lett.* **2013**, *13*, 5013–9.
- (45) Holt, J. K.; Park, H. G.; Wang, Y.; Stadermann, M.; Artyukhin, A. B.; Grigoropoulos, C. P.; Noy, A.; Bakajin, O. Fast Mass Transport through Sub-2-Nanometer Carbon Nanotubes. *Science* **2006**, *312*, 1034–7.
- (46) Kannam, S. K.; Todd, B.; Hansen, J. S.; Daivis, P. J. How Fast Does Water Flow in Carbon Nanotubes? *J. Chem. Phys.* **2013**, *138*, 094701.
- (47) Maali, A.; Cohen-Bouhacina, T.; Kellay, H. Measurement of the Slip Length of Water Flow on Graphite Surface. *Appl. Phys. Lett.* **2008**, 92, 053101.
- (48) Wang, M. C.; Chun, S.; Han, R. S.; Ashraf, A.; Kang, P.; Nam, S. Heterogeneous, Three-Dimensional Texturing of Graphene. *Nano Lett.* 2015, 15, 1829–1835.
- (49) Park, H.; Lim, C.; Lee, C.-J.; Kang, J.; Kim, J.; Choi, M.; Park, H. Optimized Poly (methyl Methacrylate)-Mediated Graphene-Transfer Process for Fabrication of High-Quality Graphene Layer. *Nanotechnology* **2018**, *29*, 415303.
- (50) Li, Z.; Wang, Y.; Kozbial, A.; Shenoy, G.; Zhou, F.; McGinley, R.; Ireland, P.; Morganstein, B.; Kunkel, A.; Surwade, S. P. Effect of Airborne Contaminants on the Wettability of Supported Graphene and Graphite. *Nat. Mater.* **2013**, *12*, 925–931.
- (51) Hurst, J. M.; Li, L.; Liu, H. Adventitious Hydrocarbons and the Graphite-Water Interface. *Carbon* **2018**, *134*, 464–469.
- (52) Hutter, J. L.; Bechhoefer, J. Calibration of Atomic-Force Microscope Tips. *Rev. Sci. Instrum.* **1993**, *64*, 1868–1873.
- (53) Neto, C.; Craig, V. S. Colloid Probe Characterization: Radius and Roughness Determination. *Langmuir* **2001**, *17*, 2097–2099.
- (54) Cottin-Bizonne, C.; Cross, B.; Steinberger, A.; Charlaix, E. Boundary Slip on Smooth Hydrophobic Surfaces: Intrinsic Effects and Possible Artifacts. *Phys. Rev. Lett.* **2005**, *94*, 056102.
- (55) Mullin, N.; Hobbs, J. K. A Non-Contact, Thermal Noise Based Method for the Calibration of Lateral Deflection Sensitivity in Atomic Force Microscopy. *Rev. Sci. Instrum.* **2014**, *85*, 113703.